Available online at www.sciencedirect.com
SCIENCE DIRECT
Journal of Photochemistry and Photobiology A: Chemistry 182 (2006) 158–167
Journal of Photochemistry and Photobiology A:Chemistry
www.elsevier.com/locate/jphotochem

Molecular modeling and spectroscopic studies on the binding of guaiacol to human serum albumin

Wenying He [a], Ying Li, Hongzong Si [a], Yuming Dong [a], Fenling Sheng [b], Xiaojun Yao [b], Zhide Hu [b,*]

[a] *Department of Chemistry, Lanzhou University, Lanzhou 730000, China*
[b] *Instrument Analysis of Research Center, Lanzhou University, Lanzhou, China*

Received 22 September 2005; received in revised form 9 January 2006; accepted 3 February 2006
Available online 18 April 2006

Abstract

The fluorogenic property of guaiacol was exploited for the first time to analyze the interaction with target protein as a probe by molecule modeling, fluorescence, Fourier transform infrared spectroscopy (FT-IR), and circular dichroism (CD) spectroscopy. Molecular docking was performed to reveal the possible binding mode or mechanism, suggested that guaiacol can strongly bind to human serum albumin (HSA) and the primary binding site of guaiacol is located in site I of HSA. It is considered that guaiacol binds to site I (subdomain II) mainly by a hydrophobic interaction and there is a hydrogen bond interactions between the drug and the residues Ala 291, which is good agreement with the results from the experimental thermodynamic parameters (the enthalpy change ΔH° and the entropy change ΔS° were calculated to be 104.008 kJ/mol and 0.409 J / mol K according to the van't Hoff equation). Data obtained by the fluorescence spectroscopy indicated that binding of guaiacol with HSA leads to dramatic enhancement in the fluorescence emission intensity along with significant occurrence of efficient Förster type resonance energy transfer (FRET) from HSA to the protein bound guaiacol. From the high value of fluorescence anisotropy ($r = 0.40$) it is argued that the probe molecule is located in motionally restricted environment of the protein. The binding constants for the interaction of guaiacol with HSA have been evaluated from relevant fluorescence data. The alterations of protein secondary structure in the presence of guaiacol in aqueous solution were quantitatively calculated by the evidences from FT-IR and CD spectroscopes.

Keywords: Guaiacol; Human serum albumin; Molecule modeling; Fourier transform infrared (FT-IR) spectroscopy; Secondary structure; Circular dichroism (CD); Fluorescence anisotropy

1. Introduction

Catechols are widespread in the environment, especially as constituents of edible plants. A lot of these catechols may undergo oxidative metabolism to electrophilic *o*-quinones by oxidative enzymes such as cytochrome P450 and peroxidases [1]. Catechol and its derivatives are important chemicals that are used in the manufacture of synthetic flavours such as vanillin [2] and are used as precursors for pharmaceutical production. They are difficult to synthesize chemically. Some microorganisms are known to produce catechols [3–6]. Catechol and its derivatives are also key metabolic intermediates in the aerobic degradation of aromatic hydrocarbons by bacteria. Catechol dioxygenases thus play a major role in the metabolism of aromatic hydrocarbons [7,8]. Recently, many studies focused on 3-methylcatechol and 4-methylcatechol [9–13]. However, till date, very little is known about *orth*-methylcatechol. *Orth*-methylcatechol (Scheme 1, named guaiacol; *o*-hydryoxyanisol or *o*-methoxyphenols), one of the active components isolated from some higher plants, has been shown to possess significant antibacterial, anti-inflammatory activities and has been clinically used to treat respiratory disease. Higher plants also possess a large set of the classical guaiacol peroxidases. These enzymes have been implicated in a wide array of physiological processes such as H_2O_2 detoxification, auxin catabolism and lignin biosynthesis and stress response (wounding, pathogen attack, etc.) [14]. In view of the pharmacological interest in the compound and the possible nutritional benefit it is imperative

* Corresponding author. Tel.: +86 931 8912540; fax: +86 931 8912582.
E-mail address: huzd@lzu.edu.cn (Z. Hu).

1010-6030/$ – see front matter © 2006 Elsevier B.V. All rights reserved.
doi:10.1016/j.jphotochem.2006.02.004

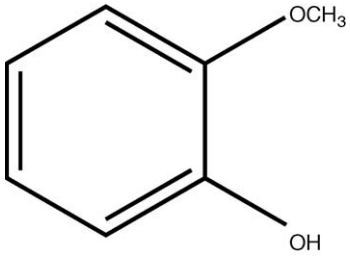

Scheme 1. The structure of guaiacol.

that the molecular mechanisms of their biological activities be analyzed. Especially it is necessary to investigate the mode of the interactions of the compound with its respective target proteins at the molecular level, so it can provide a molecular basis for elucidating the mechanism of drug acting and predicting unfavorable drug interaction. In the present paper, the experimental information on the location and nature of binding of Guaiacol to human serum albumin has been reported the first time.

Human albumin (66.5 kDa) as one of the most abundant protein in blood serum with a concentration of ca. 0.63 mM, is synthesized in the liver and exported as a non-glycosylated protein. It is a single polypeptide chain of 585 amino acids with a largely-helical (≈67%) triple-domain structure that assemble to form a heart-shaped molecule. Other mammalian albumins are highly homologous with human albumin, all of which contain 17 disulfide bridges. HSA binds a number of the relatively insoluble endogenous compounds such as unesterified fatty acids, bilirubin and bile acids and thus facilitates their transport throughout the circulation. HSA is also capable of binding a wide variety of drugs and xenobiotics [15–17]. The majority of these drug-binding studies involving HSA have shown that the distribution, free concentration and the metabolism of various drugs can be significantly altered as a function of their binding constants to HSA. He and Carter have reported that HSA has a limited number of binding sites for endogenous and exogenous ligands that are typically bound reversibly and have binding constants 10^4–10^8 [16,17].

In the previous papers we reported optical spectroscopic studies designed to characterize the interaction of active components of some Chinese herbs with human serum albumin [18,19]. And we also explored the binding of the drugs to HSA with molecular modeling tools. Docking of these drugs to the protein was performed on different groups within site I or site II. However, these studies are based on investigating the fluorescence quenching of HSA and thus induced the second structure changes of the protein. In the present paper, we demonstrated a new array on the interaction of guaiacol with HSA by the fluorescence enhancing and fluorescence polarization techniques in combination with circular dichroism (CD), Fourier transform infrared (FT-IR), UV–vis spectroscopic methods at three temperatures under physiological conditions. The partial binding parameters of the reaction were calculated through SGI FUEL workstations. Attempts were made to investigate the binding mechanism of guaiacol to HSA with respect to the binding constants, the binding sites, the thermodynamic functions and the effect of the protein secondary structure. The experimental result of the fluorescence polarization was used to study more optical characters of the protein. These are the first spectroscopic results on guaiacol–HSA interactions and they can illustrate the nature of guaiacol-protein complications in vitro and in vivo.

2. Materaials and methods

2.1. Materials

Guaiacol was of analytical grade, and purchased from the National Institute for Control of Pharmaceutical and Bioproducts, China, and the stock solution was prepared in ethanol. Human serum albumin (HSA, fatty acid free <0.05%) purchased from Sigma Chemical Co. and used without further purification. All HSA solution was prepared in the pH 7.40 buffer solution, and HSA stock solution was kept in the dark at 4 °C. Buffer (pH 7.40) consists of Tris (0.2 mol/L and HCl (0.1 mol/L), and the pH was adjusted to 7.40 by 0.5 mol/L NaOH when the experiment temperature was higher than 296 K. The pH was checked with a suitably standardized pH meter. All reagents were of analytical reagent grade and double distilled water was used throughout the experiment.

2.2. Molecule modeling

The potential of the 3D structures of HSA was assigned according to the Amber 4.0 force field with Kollman-all-atom charges. The initial structures of all the molecules were generated by molecular modeling software Sybyl 6.9 [20]. The geometries of this drug were subsequently optimized using the Tripos force field with Gasteiger-Marsili charges. The AutoDock 3.05 program 21, 22 was used to calculate the interaction modes between the drug and HSA. Lamarckian genetic algorithm (LGA) implemented in Autodock was applied to calculate the possible conformation of the drug that binds to the protein. During docking process, a maximum of 10 conformers was considered for the drug. The conformer with the lowest binding free energy was used for further analysis. All calculations were performed on SGI FUEL workstation.

2.3. Spectroscopic measurements

The absorption and steady state fluorescence measurements were performed using a Cintra-10 e UV–vis spectrometer (GBC, Australia) and a RF-5301PC spetrofluorophotometer (Shimadzu), respectively. The fluorescence emission spectra were recorded from 270 to 500 nm (excitation wavelength 295 nm) using 5/5 nm slit widths. Synchronous fluorescence spectra of HSA in the absence and presence of increasing amount of guaiacol ((0–1.33) × 10^{-5} mol/L) were recorded λ_{ex}: 290–500 nm.

Fluorescence titration experiments: 3.0 mL solution containing appropriate concentration of HSA was titrated manually by successive additions of a 1.0 × 10^{-3} mol/L methanol

stock solution of guaiacol (to give a final concentration of (0.55–5.5) × 10^{-6} mol/L) with trace syringes, and the fluorescence intensity was measured (excitation at 274 nm and emission at 308 nm). All experiments were measured at three temperatures (298, 308, and 318 K). The temperature of sample was kept by recycle water throughout experiment. For the anisotropy measurements the excitation and emission band widths were both 5 nm. Steady state anisotropy, r, is defined by [21]:

$$r = (I_{VV} - GI_{VH})/(I_{VV} + 2GI_{VH}) \quad (1)$$

where I_{VV} and I_{VH} are the intensities obtained with the excitation polarizer oriented vertically and the emission polarizer oriented in vertical and horizontal orientation, respectively. The G factor is defined as: $G = I_{HV}/I_{HH}$, I refers to the similar parameters as mentioned above for the horizontal position of the excitation polarizer.

FT-IR measurements were made at room temperature on a Nicolet Nexus 670 FT-IR spectrometer (America) equipped with a Germanium attenuated total reflection (AIR) accessory, a DTGS KBr detector and a KBr beam splitter. All spectra were taken via the Attenuated Total Reflection (ATR) method with resolution of 4 cm^{-1} and 60 scans. Spectra processing procedures: spectra of buffer solution were collected at the same condition. Then, subtract the absorbance of buffer solution from the spectra of sample solution to get the FT-IR spectra of proteins. The subtraction criterion was that the original spectrum of protein solution between 2200 and 1800 cm^{-1} was featureless [22]. In this study Fourier self-deconvolution and secondary derivative were applied to these two ranges, respectively to estimate the number, position and width of component bands in the region of 1700–1600 cm^{-1}. Based on these parameters curve-fitting process was carried out by Galactic Peaksolve software (version 1.0) to get the best Gaussian-shaped curves that fit the original protein spectrum. The component bands of amide I were attributed according to the well-established assignment criterion [23]. The bands range 1650–1660 cm^{-1} are generally assigned to α-helix, 1610–1640 cm^{-1} to β-sheet, 1640–1650 cm^{-1} to random coil, and 1660–1700 cm^{-1} to β-turn structure. The area of all the component bands assigned to a given conformation are then summed up and divided by the total area. Thus, the content of each secondary structure of HSA is calculated by area of their respectively component bands.

Circular dichroism (CD) measurements were carried out on a Jasco-20 automatic recording spectropolarimeter (Japan) in cell of pathlength 2 mm at room temperature. The induced ellipticity was obtained by the ellipticity of the drug–HSA mixture subtracting the ellipticity of drug at the same wavelength and is expressed in degrees. The results are expressed as mean residue ellipticity (MRE) in deg cm^2/dmol, which is defined as [MRE θ_{obs} (m deg)/10 nlCp]. The θ_{obs} represents the CD in millidegree, n is the number of amino acid residues (585), l the path length of the cell and Cp is the mole fraction. The α-helical content of HSA was calculated from the MRE value at 208 nm using the equation α% helix = [(MRE208-4000)/33000–4000] × 100 as described by Khan et al. [24].

3. Results and discussion

3.1. Molecular modeling

The application of molecular modeling by computer methods has been employed to improve the understanding of the interaction of guaiacol and HSA. Descriptions of 3D structure of crystalline albumin have revealed that human serum albumin comprises of three homologous domains that assemble to form a heart-shaped molecule. HSA is monomeric but contains the three structurally similar α-helical domains (I-III); each domain has two subdomains (A and B), which are six (A) and four (B) α-helices, respectively. The principal regions of ligand binding to HSA are located in hydrophobic cavities in subdomains IIA and IIIA, which are consistent with site I and site II, respectively, and one tryptophan residue (Trp-214) of HSA is in subdomain IIA. Several studies have shown that HSA is able to bind many ligands in several binding sites [17]. The crystal structure of HSA in complex with R-warfarin was taken from the Brookhaven Protein Data Bank (entry codes 1h9z). The potential of the 3D structure of HSA was assigned according the Amber 4.0 force field with Kollman-all-atom charges. The initial structure of all the molecules was generated by molecular modeling software Sybyl 6.9 [20]. The geomertries of these compounds were subsequently optimized using the Tripos force field with Gasteiger-Marsili charges. FlexX program was applied to calculate the possible conformation of the ligands that binds to the protein. The conformer with RMS (root-means-square) was used for further analysis. Based on this kind of approach a computational model of the target receptor has been built, partial binding parameters of the guaiacol–HSA system were calculated through SGI FUEL workstations. The best energy ranked results of the binding mode between guaiacol and HSA is shown in Fig. 1, only residues around 8 Å of guaiacol is displayed. As shown in Fig. 1, guaiacol binds within the subdomain IIA of the protein (The Warfarin Binding Pocket). The phenolic moiety is located within the binding pocket and the ring and methyoxyl-fraction are no coplanar. It is important to note that the residues of HSA Alg222 and (Lys199) are in close proximity to the methyoxyl-fraction of guaiacol suggesting the existence of hydrophobic interaction between them. On the other hand, there is the hydrogen interaction between OH of guaiacol and the residues Ala291 of HSA. The results indicated that the formation of hydrogen bond decreased the hydrophilicity and increase the hydrophobicity to stability the guaiacol–HSA system. The amino acid residues with benzene ring can match that of the guaiacol in space in order to firm the conformation of the complex. But the interaction between guaiacol and HSA is not exclusively hydrophobic in nature since there are several polar residues in the proximity of the bound ligand (shown in arrows), which play a subordinate role in stabilizing the drug molecule via electrostatic interaction, which is also in agreement with the binding mode study. The calculated binding Gibbs free energy (ΔG) is −13.32 kJ/mol, which are close to the experimental data (−17.01 kJ/mol). However, the results obtained from modeling indicated that the interaction between guaiacol and HSA is dominated by hydrophobic force, and there is also a hydro-

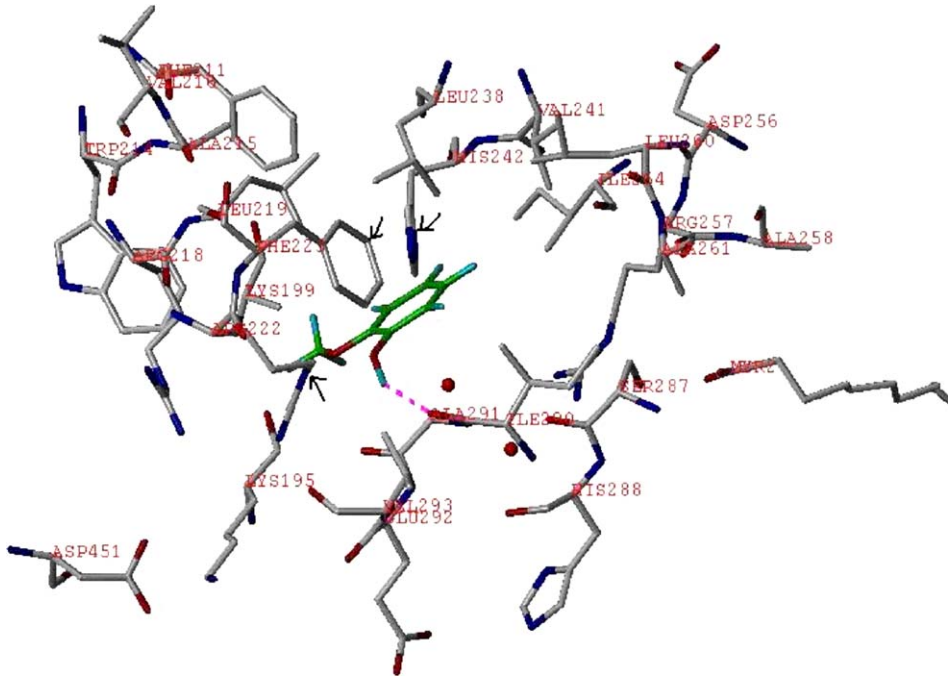

Fig. 1. The binding mode between guaiacol and HSA, only residues around 8 Å of guaiacol is displayed. The residues of HSA are represented using line and the guaiacol structure is represented using ball and stick model. The hydrogen bond between guaiacol and HSA is represented using dashed line.

gen bond between the drug and the polar amino acid residues Ala291.

3.2. Binding studies using fluorescence and UV–vis spectroscopy

In an attempt to investigate the binding of guaiacol to HSA, fluorescence titration was used. The room temperature emission spectrum of guaiacol in Tris buffer shows an unstructured band with a maximum at around 308 nm with an enhancement in the fluorescence intensity (Fig. 2). The interaction of guaiacol to HSA and the conformation changes in HSA were evaluated by measuring the intrinsic fluorescence intensity of protein before and after addition of guaiacol. Fig. 3 shows the fluorescence emission spectra of HSA in presence of increasing concentrations of guaiacol. It is evident that addition of drug causes a dramatic enhancement in the fluorescence emission intensity of HSA accompanied by conspicuous changes in its emission profile. In presence of guaiacol we observe dual fluorescence emission with peaks occurring at 307 and 311 nm, respectively. A remarkable blue shift of the maximum emission wavelength was also observed, which is ascribed to a lowering in the polarity of the protein environment compared to that of the pure protein solution [25]. And the structureless behavior of the emission

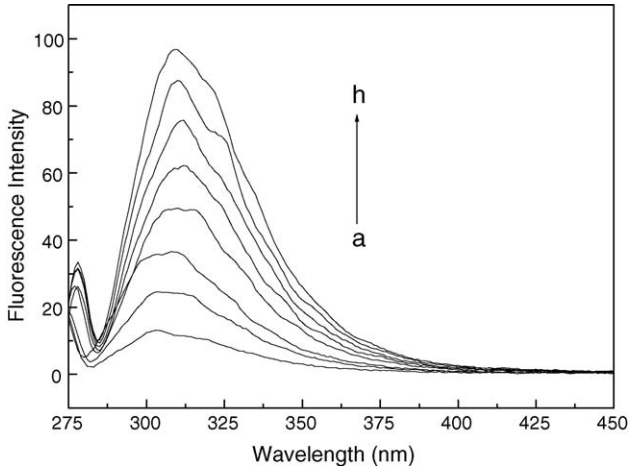

Fig. 2. The fluorescence emission spectrum of free guaiacol. The concentration of the guaiacol concentration is corresponding to 0.55; 1.10; 1.65, 2.20; 2.75; 3.30, 3.85, 4.40 × 10^{-6} mol/L from the (a) to the (h); T = 298 K, pH 7.40; λ_{ex} = 274 nm.

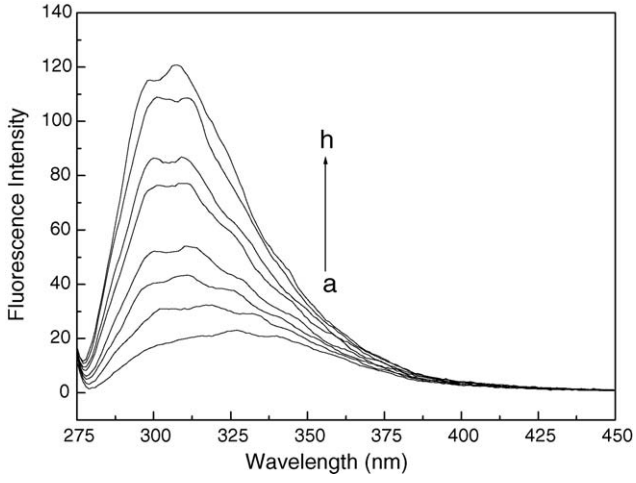

Fig. 3. The fluorescence spectra of guaiacol–HSA system. The concentration of HSA was 1.5 × 10^{-6} mol/L while the guaiacol concentration corresponding to 0, 0.55; 1.10; 1.65, 3.30; 3.85; 4.95, 5.50 × 10^{-6} mol/L from the (a) to the (h); T = 298 K, pH 7.40; λ_{ex} = 274 nm, λ_{em} = 308 nm.

spectra with the addition of guaiacol in Tris buffer solution can be rationalized in terms of binding of the probe with the protein leading to a less polar microenvironment around the fluorophore. One the one hand, substitution with electron-donating groups (−OH, OCH_3) of guaiacol induces an increase in the molar absorption coefficient and a shift in both absorption and fluorescence spectra. A significant intramolecular charge transfer character of the relevant transitions is expected for planar aromatic phenol; this is confirmed by the fact that the fluorescence spectra are broad and structureless. Another reasonable explains comes from the theory about the red-edge effects [26]. The width of a band in the emission spectrum of fluorophore located in a particular microenvironment is a result of two effects: homogeneous and inhomogeneous broadening. In most cases, the extent of inhomogeneous broadening is much greater than that of homogeneous broadening. When interactions with the surrounding molecules are strong, and many configurations are possible, the spectra may become completely changed. This phenomenon might be the result of the radiation less energy transfer between guaiacol and HSA. In our work, it is clear that the emission spectrum were belonged to the inhomogeneous broadening, which suggested that the microenvironment around HSA is changed after the addition of guaiacol. The results were also confirmed by the absorption spectrum of guaiacol–HSA in Tris buffer at pH 7.40 (Fig. 4). It shows a broader and an increase absorbance intensity band with a maximum at around 204 nm and a slight shift to long wavelength. Thus, the evidences from fluorescence and UV spectra indicated that the interaction of guaiacol and HSA bring about the microenvironment change around HSA.

In order to see the interaction between the drug and the protein, the binding constant value was determined from the fluorescence intensity considering the following equation as developed by Bhattacharya et al. [27].

$$1/\Delta F = 1/\Delta F_{max} + (1/K[Q])/(1/\Delta F_{max}) \quad (2)$$

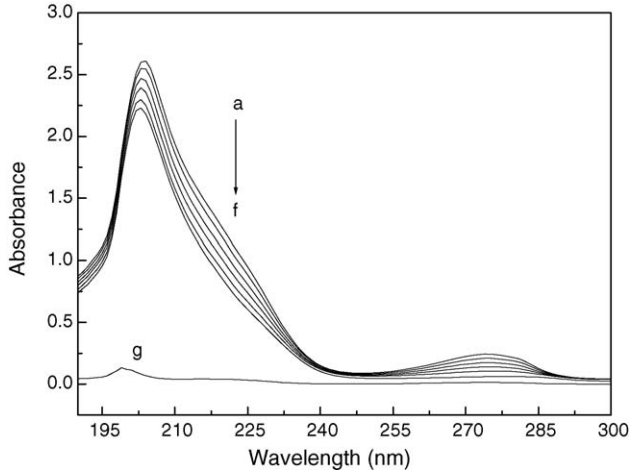

Fig. 4. UV absorption spectra of HSA in Tris buffer solution in presence of different guaiacol concentrations: (a) 5.50×10^{-6} mol/L, (b) 4.40×10^{-6} mol/L, (c) 3.30×10^{-6} mol/L, (d) 2.20×10^{-6} mol/L, (e) 1.10×10^{-6} mol/L, (f) 0; [HSA] = 1.5×10^{-6} mol/L; (g) the spectra of guaiacol, 1.10×10^{-6} mol/L, 298 K.

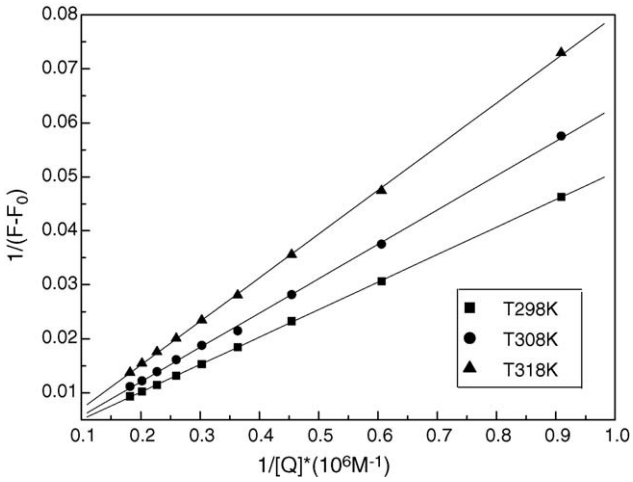

Fig. 5. Plot of $1/(F–F_0)$ against 1/[Q]. λ_{ex} = 274 nm, λ_{em} = 308 nm.

where $\Delta F = F_\chi – F_0$ and $\Delta F_{max} = F_\infty – F_0$ where F_0, F_χ and F_∞ are the fluorescence intensities of HSA in the absence of guaiacol, at an intermediate concentration of guaiacol, and at the saturation of interaction, respectively; K being the binding constant and $[Q]$, the drug concentration. The linearity in the plot of $1/(F–F_0)$ against $1/[Q]$ confirms a one-to-one interaction between the two partners (Fig. 5). The binding constants at three temperatures (298, 308 and 318 K) are shown in Table 1 and used to calculate the thermodynamics parameters.

Fluorescence polarization (FP) is a powerful and sensitive technique for the study of molecular interactions in solution. FP is based on the observation of the molecular movement of the fluorescent molecules in solution and does not require physical separation of the excess ligand or acceptor [28]. Small fluorescent molecules have low polarization values, while large molecules caused by binding of other molecules have higher ones [29]. Figs. 6 and 7 represent the variations of fluorescence anisotropy (r) of the emission of HSA as a function of guaiacol concentration and that of the emission of guaiacol as a function of HSA concentration, respectively. Both of the plots show the marked decrease in the fluorescence anisotropy of the fluorophore to HSA environment. The gradual decrease in the anisotropy value indicates an interaction between guaiacol and HSA. The high anisotropy values (r = 0.24 at [HSA] = 1.5 μM for Fig. 6; r = 0.40 at [Guaiacol] = 1.65 μM for Fig. 7) suggest that the probe molecules are bound in a motionally restricted environment introduced by HSA. It further suggests that the rotational diffusion of the probe is unconstrained significantly in the protein medium. With the addition of HSA (λ_{ex} = 295 nm), attainment of the plateau in Fig. 7

Table 1
Binding constant (K), and thermodynamic parameters for the binding of guaiacol to HSA

Temperature (K)	K ($\times 10^4$)	ΔG (kJ/mol)	ΔS (J/mol K)	ΔH (kJ/mol)
298	0.956	−17.00	0.41	104.01
308	1.086	−23.80	0.41	104.01
318	1.310	−25.06	0.41	104.01

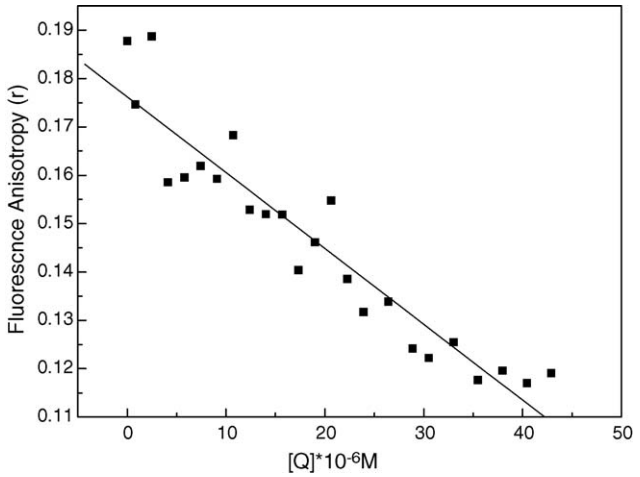

Fig. 6. Variation in the fluorescence anisotropy (r) of HSA (1.5 μM) with increasing guaiacol concentration (λ_{ex} = 296 nm, λ_{em} = 330 nm).

implies saturation in the binding interaction between the two partners.

3.3. Binding mode

It is well known that the fluorescence of HSA comes from the tyrosine, tryptophan, and phenylalanine residues. According to Miller [30], with large $\Delta\lambda$ values such as 60 nm, the synchronous fluorescence of HSA is characteristic of tryptophan residue. Fig. 8 shows the effect of addition of guaiacol on the synchronous fluorescence spectrum of HSA when $\Delta\lambda$ = 60 nm. The addition of the drug results in the fluorescence enhancement with the maximum emission wavelength at 338–328 nm. It is reported that the maximum emission wavelength (λ_{max}) at 330–332 indicated that trytophan resides are located in the non-polar region, i.e., they are buried in a hydrophobic cavity in HSA; λ_{max} at 350–352 nm shows that tryptophan residues are exposed to water, i.e., the hydrophobic cavity in HSA is disagglomerated and the structure of HSA is looser. Thus Fig. 8 suggests that guaiacol mainly bound to the hydrophobic cavity

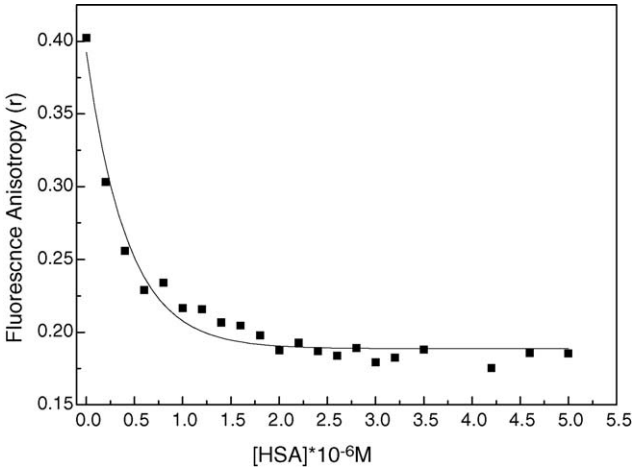

Fig. 7. Variation in the fluorescence anisotropy (r) of guaiacol (1.65 μM) with increasing protein (HSA) concentration (λ_{ex} = 296 nm, λ_{em} = 330 nm).

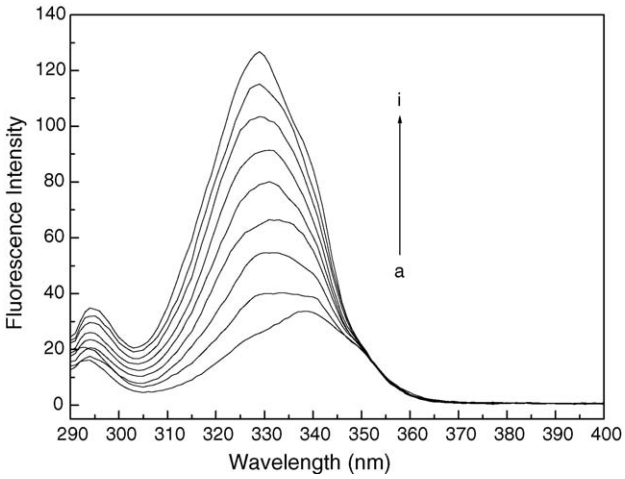

Fig. 8. Synchronous fluorescence spectra of HSA (1.5 μM) with $\Delta\lambda$ = 60 nm in the absence and presence of increasing amount of guaiacol (μM) from 0 to 5.5 from the (a) to the (i). Tris buffer, pH 7.4, 298 K.

of HSA, which is in accordance with the results from molecular modeling and the thermodynamics parameters obtained by the experimental data as follows.

The molecular forces contributing to protein interactions with small molecular substrates may be a van'der Waals interaction, Hydrogen bonds, ionic, electrostatic and hydrophobic interactions, etc. The signs and magnitudes of thermodynamic parameters for protein reactions can be account for the main forces contributing to protein stability. If the enthalpy changes (ΔH°) does not vary significantly over the temperature range studied, then its value and that of ΔS° can be determined from the van't Hoff equation:

$$\ln K = -\Delta H^\circ/RT + \Delta S^\circ/R \quad (3)$$

$$\Delta G^\circ = \Delta H^\circ - T\Delta S^\circ \quad (4)$$

In Eq. (3), K is the binding constant at corresponding temperature and R is the gas constant. The enthalpy change (ΔH°) calculated from the slope of the van't Hoff relationship. The free energy change ΔS° is estimated from Eq. (4). Thus, the thermodynamic parameters were obtained from the relationship between ln K and the reciprocal absolute temperature. According to the binding constants of guaiacol to HSA obtained at the three temperatures (298, 308 and 318 K), the thermodynamic parameters were determined from linear van't Hoff plot (not shown) and presented in Table 1. As shown in Table 1, ΔH° and ΔS° for the binding reaction between guaiacol and HSA are found to be 104.008 kJ/mol and 0.409 J/mol K. Thus, the formation of guaiacol–HSA coordination compound is an exothermic reaction accompanied by positive ΔS° value. Ross and Subramanian [31] have characterized the sign and magnitude of the thermodynamic parameter associated with various individual kinds of interaction that may take place in protein association processes, as described below. From the point of view of water structure, a positive ΔS° value is frequently taken as typical evidence for hydrophobic interaction. Furthermore, specific electrostatic interactions between ionic species in aqueous solution are characterized by a positive value of ΔS° and a negative ΔH° value,

while negative entropy and enthalpy changes arise from van der Waals forces and hydrogen formation in low dielectric media. Accordingly, it is not possible to account for the thermodynamic parameters of guaiacol–HSA coordination compound on the basis of a single intermolecular force model. Therefore, the binding of guaiacol to HSA might involve hydrophobic interaction strongly as evidenced by the positive values of ΔS° and the electrostatic interaction can also not be excluded. Meanwhile, it is found that the major contribution to ΔG° arise from the ΔH° term rather than from ΔS°, so the binding process is enthalpy driven, and the increase of entropy might be based on the destruction of the iceberg structure induced by the hydrophobic interaction. Under the conditions studied, the negative charge densities (δ) of guaiacol were calculated under the simulative physiological condition (pH 7.40) using the spectrophotometric method [32]. For the guaiacol–HSA system, guaiacol is nearly unionized under the experimental conditions (pH 7.40) in view of its pK_{α} value (shown in Table 2); so electrostatic interactions can be precluded from the binding process because of the small negative charge density on them. The evidences from Table 2 indicated that with the increases of guaiacol concentration, the dissociation constants (K_a) decreased and the values of δ increased, respectively. However, the above results in combination with the synchronous fluorescence evidences were good well agreement with the information coming from molecular modeling. That is to say, the hydrophobic interaction might play a major role in the binding guaiacol to HSA.

3.4. Energy transfer between guaiacol and HSA

Förster's theory of dipole–dipole energy transfer was used to determined the distances between the protein residue (donor) to the bound drug (acceptor) in HSA. By Förster's theory [33], the efficiency of energy transfer (E) is related to the distance R (Å) between donor and acceptor by:

$$E = 1 - \Phi/\Phi_0 = R_0^6/(R_0^6 + r^6) \quad (5)$$

R_0, the distance (Å) at which the transfer efficiency equals to 50%, is given by the following equation:

$$R_0^6 = 8.8 \times 10^{-25}\kappa^2\Phi_d\eta^{-4}\int F(\lambda)\varepsilon(\lambda)\lambda^4\,d\lambda / \int F(\lambda)\,d(\lambda) \quad (6)$$

where η is the refractive index of the medium, κ^2 the orientation factor, Φ_d the quantum yield of the donor; $F(\lambda)$ the fluorescence intensity of the fluorescence reagent when the wavelength is λ, $\varepsilon(\lambda)$ the molar absorbance coefficient of the acceptor at the wavelength of λ. From these relationships, E and R_0 can be calculated; so the value of r, also can be calculated. Fig. 9 is the overlap of the fluorescence spectra of HSA and the absorption spectra of the drug. Under these experimental conditions, it has been reported for HSA that, $K^2 = 2/3$, $\Phi = 0.14$, $n = 1.36$ [34]. So the value of the spectral overlap integral between the donor emission spectrum and the acceptor absorbance spectrum was calculated from Fig. 9, the value of R_0 is 2.08 nm and the r is 2.12 nm, respectively. Obviously, they are lower than 7 nm after interaction between the drugs and HSA. This result according with conditions of Föster's theory indicated the non-radiative energy transfer between guaicol and HSA.

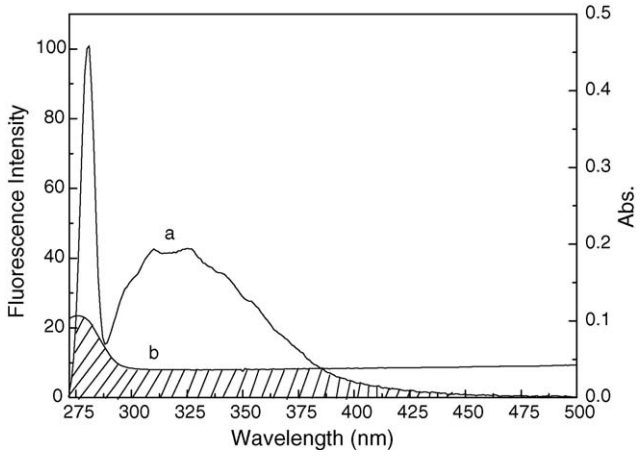

Fig. 9. Overlapping between the fluorescence emission spectrum of HSA (a) ($\lambda_{ex} = 274$ nm) and absorption UV spectrum of guaiacol (b). $C_{drug}/C_{HSA} = 1{:}1$. $T = 296$ K.

3.5. Changes of the protein's secondary structure induced by drug-binding

Because our molecular docking attempts to address how guaiacol binding to HSA, it is important to examine how the structure of HSA is affected by this conformational change. When drugs bind to a globular protein, the intramolecular forces responsible for maintaining the secondary and tertiary structures can be altered, resulting in a conformational change of the protein [17]. The distinct fluorescence enhancement suggested that the drug–HSA combination has changed the microenvironment of HSA. The blue shifts of fluorescence emission wavelength, shown in Fig. 3, also indicated that the conformation has been changed after protein binding with guaiacol. If the change of protein structure included the transforming of protein secondary structure in the drug–HSA complex, it can be reflected in the infrared absorption spectra or CD spectra.

Since infrared spectra of proteins exhibit a number of so-called amide bands which represent different vibrations of the peptide moiety. Of all the amide modes of the peptide group, the single most widely used one in studies of protein secondary structure is the amide I. This vibration mode originates from

Table 2
Variation in the parameters of fluorescence and physical properties in Tris buffer, T298 K, pH 7.40

[Guaiacol] μM	0.00	0.55	1.10	1.65	2.20	2.75	3.30	3.85	4.40	4.95	5.50
pK_{α} (Dissociatin constants)		9.13	8.89	8.63	8.51	8.42	8.34	8.27	8.22	8.18	8.15
δ (Charge density)		0.02	0.03	0.05	0.07	0.09	0.11	0.12	0.13	0.14	0.150

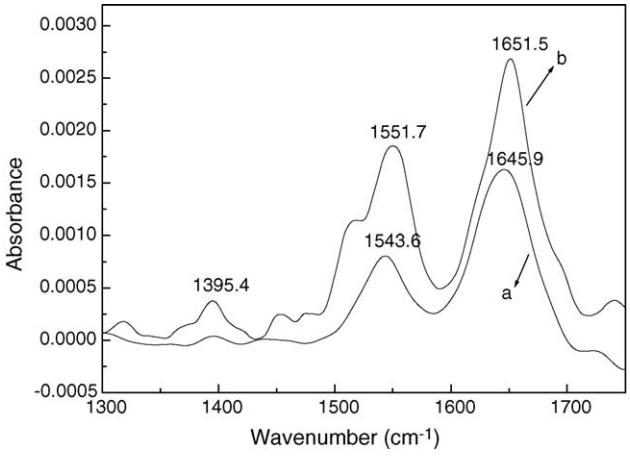

Fig. 10. FT-IR spectra and different spectra of HSA in aqueous solution (a) FT-IR spectrum of HSA; (b) FT-IR difference spectrum of HSA obtained by subtracting the spectrum of the guaiacol-free form from that of the guaiacol-bound form in the region of 1725–1500 cm^{-1} at 298 K Tris buffer (pH 7.40) ([HSA] = 1.5×10^{-6} mol/L; [guaiacol] = 3.0×10^{-6} mol/L).

the C=O stretching vibration of the amide group (coupled to the in-phase bending of the N–H bond and the stretching of the C–N bond) and gives rise to infrared bands in the region between approximately 1600 and 1700 cm^{-1} [35]. Fig. 10 is the FT-IR spectra of the guaiacol free and guaiacol-bound form of HSA. From Fig. 10, we concluded that the secondary structure of HSA is changed because the peak position of amide I band (1645.5 cm^{-1}) and amide II band (1543.6 cm^{-1}) in the HSA infrared spectrum has an evident shift and their peaks shape are also changed. Fig. 11 showed a quantitative analysis of the protein secondary structure of HSA before and after the interaction with guaiacol in Tris buffer. The free protein contained major amounts of α-helices (55%), β-sheets (22%), β-turn structures (11%), and β-antiparallels (12%) [36]. Table 3 lists the curve-fitted results of protein secondary structure before and after binding with different concentration of drugs. From Table 3, it can be seen that the percentage of protein α-helix structure decreased about 17.6% and β-turn structure increased about 29.6%, but β-sheet structure showed a very slight change.

Additional evidence regarding the guaiacol–HSA complications comes from CD spectroscopy results. Fig. 12 shows the CD spectra of the HSA and HAS–guaiacol complex obtained at pH 7.40. The CD spectra of HSA exhibited two negative minimum at 208 and 222 nm, which is typical characterization of the α-helix structure of class proteins. The reasonable explanation is that the negative peaks between 208 and 209 nm and 222–223 nm are both contributed to $n \rightarrow \pi^*$ transfer for the peptide bond of α-helical [37]. As shown in Fig. 12, the binding of guaiacol to HSA caused only a decrease in negative ellipticity at all wavelengths of the far-UV CD without any significant shift of the peaks, indicating that this drug induces a slight decrease in the α-helix structure content of the protein. However, the CD spectra of HSA in presence and absence of guaiacol are similar in shape, indicating that the structure of HSA is also predominantly α-helix. From the above results, it is apparent that the effect of guaiacol on HSA causes a conformational change of the protein, with the loss of helical stability. The calculating results exhibited a reduction of α-helix structures from 47.1 to 42.98% at molar ratio guaiacol/HSA of 2:1(Table 3).

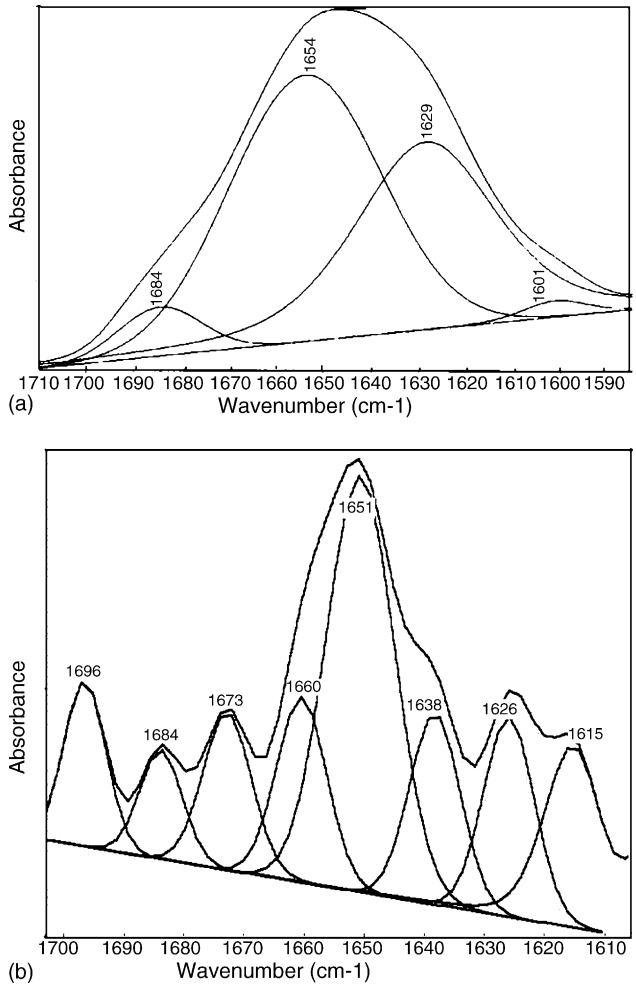

Fig. 11. Curve-fitted amide I (1700–1600) regions of free HSA (curve a) and guaiacol–HSA (curve b) in buffer solution with [HSA]/[guaiacol] = 1:2, T = 298 K, Tris buffer, pH 7.40.

Table 3
Secondary structure determination for the free HSA and its coordination compounds in Tris buffer (pH 7.40) at the molar concentration ratio: C_{drug}/C_{HSA} = 2:1; T = 298 K

	Amide I components (cm^{-1})	1660–1700 β-turn (%)	1650–1660 α-helice (%)	1610–1640 β-sheet (%)
The FT-IR results	HSA-free	6.40	54.4	39.2
	HSA + guaiacol	36.79	36.80	39.77
The CD results (α-helice %)	HAS-free		47.12	
	HAS + guaiacol		42.98	

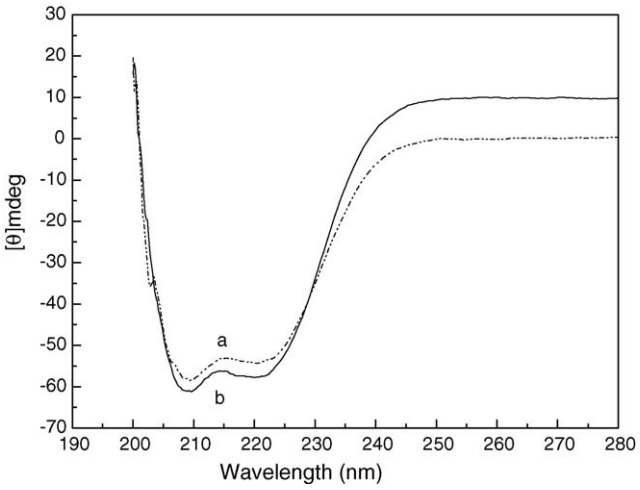

Fig. 12. CD spectra of the HAS–guaiacol system. (a) 1.5×10^{-6} mol/L HSA; (b) 1.5×10^{-6} mol/L HSA + 3.0×10^{-6} mol/L guaiacol. $T = 298$ K, Tris buffer, pH 7.40.

4. Conclusions

The interactions between guaiacol and HSA have been investigated in this work using molecular modeling and different optical techniques. The results suggested that guaiacol could bind HSA through the hydrophobic and hydrogen bond between guaiacol and ALA 291 residue. The binding site is located in the hydrophobic pocket of subdomain II A according to the molecular docking study. Experimental results also showed that the binding of guaiacol to HSA induced a conformational change of HSA, which was further proved by the quantitative analysis data of CD and FT-IR spectrum. In addition, the data of fluorescence anisotropy and quantum yield obtained indicated also the changes of microenvironment of HSA induced by the binding guaiacol.

References

[1] J.L. Bolton, E. Pisha, S. Li, E.S. Krol, L.I. Suzanne, Z.W. Huang, B.B. Richard, M.P. John, The reactivity of *o*-quinones which do not isomerize to quinone methods correlates with alkylcatechol-induced toxicity in human melanoma cells, Chem. Biol. Interact. 106 (1997) 133–148.
[2] K. Shirai, Screening of microorganisms for catechol production from benzene, Agric. Biol. Chem. 50 (1986) 2875–2880.
[3] M.D. Ennis, N.B. Ghazal, The synthesis of (+)- and (−)-flesinoxan: application of enzymatic resolution methodology, Tetrahedron Lett. 33 (1992) 6287–6290.
[4] V. Scharrenburg, G.J.M., J. Frankena, Biokatalyse helpt farmaceutische industrie bij asymmetrische synthese, Chem. Mag., 4 (1996) 284–286.
[5] M. Held, A. Schmid, H.P.E. Kohler, W. Suske, B. Witholt, M.G. Wubbolts, An integrated process for the production of toxic catechols from toxic phenols based on a designer biocatalyst, Biotechnol. Bioeng. 62 (1999) 641–648.
[6] G.K. Robinson, G.M. Stephens, H. Dalton, P.J. Geary, The production of catechols from benzene and toluene by *Pseudomonas putida* in glucose fed-batch culture, Biocatalysis 6 (1992) 81–100.
[7] B.E. Haigler, J.C. Spain, Biotransformation of nitrobenzene by bacteria containing toluene degradative pathways, Appl. Environ. Microbiol. 57 (1991) 3156–3162.
[8] D. Kima, J.C. Chae, J.Y. Jang, G.J. Zylstra, Y.M. Kim, B.S. Kang, E. Kim, Functional characterization and molecular modeling of methylcatechol 2,3-dioxygenase from *o*-xylene-degrading Rhodococcus sp. strain DK17, Biochem. Biophys. Res. Commun. 326 (2005) 880–886.
[9] M.E. Kauffman, W.K. Keener, S.R. Clingenpeel, M.E. Watwood, D.W. Reed, Y. Fujita, R.M. Lehman, Use of 3-hydroxyphenylacetylene for activity-dependent, fluorescent labeling of bacteria that degrade toluene via 3-methylcatechol, J. Microbiol. Meth. 55 (2003) 801–805.
[10] L.E. Husken, M. Oomes, K. Schroen, J. Tramper, J.A.M. de Bont, R. Beeftink, Membrane-facilitated bioproduction of 3-methylcatechol in an octanol/water two-phase system, J. Biotechnol. 96 (2002) 281–289.
[11] N. Callizot, J.M. Warter, P. Poindron, Pyridoxine-induced neuropathy in rats: a sensory neuropathy that responds to 4-methylcatechol, Neurobiol. Dis. 8 (2001) 626–635.
[12] A. Chiharu, T. Nakanishi, N. Sogawa, K. Ishii, N. Ogawa, M. Takigawa, H. Furuta, Stimulatory effects of 4-methylcatechol, dopamine and levodopa on the expression of metallothionein-III GIF mRNA in immortalized mouse brain glial cells VR-2 g, Brain Res. 792 (1998) 335–339.
[13] The Pharmacy Instruction of Guaiacol, The National Institute for Control of Pharmaceutical and Bioproducts, China, 2004, p. 6.
[14] M. Tognolli, C. Penel, H. Greppin, P. Simon, Analysis and expression of the class III peroxidase large gene family in Arabidopsis thaliana, Gene 288 (2002) 129–138.
[15] T. Peters, All About Albumin, Academic Press, New York, 1996 (and reference therein).
[16] J.X. He, D.C. Carter, Atomic structure and chemistry of human serum albumin, Nature 358 (1992) 209–215.
[17] U. Kragh-Hansen, Molecular aspect of ligand binding to serum albumin, Pharmacol. Rev. 33 (1981) 17–53.
[18] W.Y. He, Y. Li, J.Q. Liu, Z.D. Hu, X.G. Chen, Specific interaction of chalcone-prote: cardamonin binding site II on HSA molecule, Biopolymers 79 (2005) 48–57.
[19] Y. Li, W.Y. He, J.Q. Liu, F.L. Sheng, Z.D. Hu, X.G. Chen, Binding of the bioactive component Jatrorrhizine to human serum albumin, Biochim. Biophy. Acta 1722 (2005) 15–21.
[20] SYBYL Software, Version 6.9, Tripos Associates Inc., St. Louis, 2002.
[21] J.R. Lakowicz, Principles of Fluorescence Spectroscopy, Plenum, New York, 1983, pp. 341–379.
[22] A.C. Dong, P. Huang, W.S. Caughey, Protein secondary structure in water from second-derivative amide I infrared spectra, Biochemistry 29 (1990) 3303–3308.
[23] K.W. Surewicz, H.H. Mantsch, New insight into protein secondary structure from resolution-enhanced infrared spectra, Biochim. Biophys. Acta 952 (1988) 115–130.
[24] A.M. Khan, S. Muzammil, J. Musarrat, Differential binding tetracyclines with serum albumin and induced structural alterations in drug-bound protein, Int. J. Biol. Macromol. 30 (2002) 243–249.
[25] A. Mallick, S. Maity, B. Haldar, P. Purkayastha, N. Chattopadhyay, Photophysics of 3-acetyl-4-oxo-6,7-dihydro-12H indolo-[2,3-a]quinolozine: emission from two states, Chem. Phys. Lett. 371 (2003) 688–693.
[26] Molecular Fluorescence: Principles and Applications, Bernard Valeur, Wiley-VCH Verlag GmbH, vol. 68, 2001, p. 56, p. 68, ISBNs: 3-527-29919-X (Hardcover), 3-527-60024-8 (Electronic).
[27] J. Bhattacharya, M. Bhattacharya, A. Chakraborty, U. Chowdhury, R.K. Podder, Interaction of chlorpromazine with mioglobin and hemoglobin. A comparative study, Biochem. Pharmacol. 47 (1994) 2049–2052.
[28] J.J. Hill, C.A. Royer, in: L. Brand, M.L. Johnson (Eds.), Methods in Enzymology, vol. 278, Academic Press, San Diego, 1997, pp. 390–416.
[29] K. Chisachi, S. Murano, M. Tsuruoka, Rapid and simple detection of PCR product DNA: a comparison between Southern hybridization and fluorescence polarization analysis, Gene 259 (2000) 123–127.
[30] J.N. Miller, Recent advances in molecular luminescence analysis, Proc. Anal. Div. Chem. Soc. 16 (1979) 203–208.
[31] P.D. Ross, S. Subramanian, Thermodynamic of protein association reactions: forces contributing to stability, Biochemistry 20 (1981) 3096–3102.
[32] Analytical Chemistry, 1st ed., Wuhan University, People Press, 1978, pp. 131–132.
[33] L. Stryer, Fluorescence energy transfers as a spectroscopic ruler, Annu. Rev. Biochem. 47 (1978) 819–846.

[34] L. Cyril, J.K. Earl, W.M. Sperry, Biochemists Handbook, E & FN Epon Led. Press, London, 1961, p. 83.
[35] K.S. Witold, H.M. Henry, C. Dennis, Determination of protein secondary structure by Fourier transform infrared spectroscopy: a critical assessment, Biochemistry 32 (1993) 389–394.
[36] L. Boulkanz, N. Balcar, M.H. Baron, FT-IR analysis for structure characterization of albumin adsorbed on the reversed-phase support RP-C_6, Appl. Spectrosc. 49 (1995) 1346–1737.
[37] P. Yang, F. Gao, The Principle of Bioinorganic Chemistry, Science Press, 2002, p. 349.